FEBS Letters 576 (2004) 358–362 FEBS 28869

The SEP domain of p47 acts as a reversible competitive inhibitor of cathepsin L

Michael Soukenik[a,d], Anne Diehl[a,b], Martina Leidert[a], Volker Sievert[b,c], Konrad Büssow[b,c], Dietmar Leitner[a,b], Dirk Labudde[a,b], Linda J. Ball[a,1], Annette Lechner[e], Dorit K. Nägler[e], Hartmut Oschkinat[a,d,*]

[a]*Forschungsinstitut für Molekulare Pharmakologie, Robert-Rössle Str. 10, D-13125 Berlin, Germany*
[b]*Proteinstrukturfabrik, Berlin, Germany*
[c]*Max Planck Institut für Molekulare Genetik, Berlin, Germany*
[d]*Freie Universitaet Berlin, Berlin, Germany*
[e]*Department of Clinical Chemistry and Clinical Biochemistry, LMU Munich, Germany*

Received 20 July 2004; revised 13 September 2004; accepted 13 September 2004

Available online 25 September 2004

Edited by Amy McGough

Abstract The solution structure of the human p47 SEP domain in a construct comprising residues G1-S2-p47(171–270) was determined by NMR spectroscopy. A structure-derived hypothesis about the domains' function was formulated and pursued in binding experiments with cysteine proteases. The SEP domain was found to be a reversible competitive inhibitor of cathepsin L with a K_i of 1.5 μM. The binding of G1-S2-p47(171–270) to cathepsin L was mapped by biochemical assays and the binding interface was investigated by NMR chemical shift perturbation experiments.

Keywords: SEP; p97; p47; Cathepsin L; NMR; Protein structure

1. Introduction

AAA-type ATPases (ATPases associated with various cellular activities) and their binding partners form protein systems involved in the regulation of membrane fusion [1], postmitotic reassembly of the Golgi apparatus, ubiquitin-related processes and DNA replication. p97 is a member of this family, which includes the Clp family proteins and yeast CDC48 [2]. It forms a hexameric structure and contains two ATPase domains, belonging thus to the AAA+ superfamily. p97 binds a variety of proteins with various functions, for example VCIP135 (valosin-containing protein (p97)/p47 complex-interacting protein p135) [3] and p47. It is composed of three domains: an N-terminal domain N, which binds the conserved 370 residue eukaryotic adaptor protein p47 [2] followed by two ATPase binding domains called D1 and D2. Binding of p47 to p97 activates the ubiquitin-binding site in p47 and deactivates the ATPase activity of p97. Like many adaptor proteins, p47 is also characterised by a modular composition, comprising an N-terminal UBA domain [4,5], a SEP (*Saccharomyces cerevisiae*, *Drosophila melanogaster* eyes closed gene and vertebrate p47) domain and a C-terminal UBX domain. The latter consists of about 80 amino acids and adopts a ubiquitin-like-β grasp fold [6]. p47 binds to p97 by insertion of a conserved loop of its UBX domain into a hydrophobic pocket within the p97 N domain [2].

As yet unknown is the function of the SEP domain, which occurs frequently and mainly in single units. The co-occurrence of SEP and UBX domains in evolutionarily conserved combinations is also interesting. Almost all proteins containing a SEP domain are succeeded closely by a UBX domain, according to SMART [7]. The solution structure of the SEP domain from rat p47 using a construct containing residues 171–246 was recently determined by Yuan et al. [8]. It was suggested that the SEP domain is involved in the binding of p47 to p97 [8]. Here, we present the structure of the human p47 SEP domain, using an extended construct (residues 171–270). Furthermore, we have derived a novel, structure-based hypothesis about the function of the p47 SEP domain, implicating it as a reversible competitive inhibitor of the lysosomal cysteine protease cathepsin L. The binding interface of the SEP domain was investigated by NMR.

2. Materials and methods

2.1. Expression/purification

The DNA sequence encoding human p47(171–270) SEP domain (NM 016143) was cloned from a human foetal brain cDNA expression library (hEx1) [9] into the expression plasmid pQTEV (GenBank Accession No. AY243506). Construct residues 3–102 correspond to sequence positions 171–270 from human p47. Two N-terminal residues from the cloning site are referred to as G1 and S2. The SEP domain was expressed as His-tagged-fusion protein in *Escherichia coli* and purified on a MC-Poros column (Applied Biosystems) loaded with Ni^{2+}. The His tag was cleaved using TEV protease, at 4 °C, overnight. The untagged SEP domain was further purified by a final gel filtration step. Uniformly ^{15}N- and $^{13}C/^{15}N$-labelled samples of the p47 SEP

* Corresponding author. Fax: +493094793169.
E-mail address: oschkinat@fmp-berlin.de (H. Oschkinat).

[1] Present address: Structural Genomics Consortium, University of Oxford, Botnar Research Centre, OX37LD, UK.

Abbreviations: NaP_i, sodium phosphate buffer; SEP, *Saccharomyces cerevisiae* SHP1, *Drosophila melanogaster* eyes closed gene, vertebrate p47; NOE, nuclear Overhauser effect; CSP, chemical shift perturbations

0014-5793/$22.00
doi:10.1016/j.febslet.2004.09.037

domain were prepared by growing cells in minimal medium containing either 0.5 g/l $^{15}NH_4Cl$ or 0.5 g/l $^{15}NH_4Cl$ and 2 g/l ^{13}C glucose, respectively. Deuterated ^{15}N-labelled protein was prepared by growing cells in 99.8% D_2O, using non-deuterated glucose.

2.2. NMR spectroscopy/structure calculation

All NMR spectra were acquired at 300 K and recorded on a Bruker DRX 600 MHz spectrometer equipped with a cryoprobe, using the programs PASTE and PAPST [10], except for the ^{15}N-edited-HSQC which was recorded on a Bruker DMX 750 MHz spectrometer. Uniformly ^{15}N-, ^{13}C- and ^{15}N-labelled proteins with concentrations of 1 and 2 mM, respectively, in a buffer consisting of 20 mM sodium phosphate buffer (NaP_i), 150 mM NaCl and 0.02% NaN_3 at pH 5.6 in 90% H_2O/10% D_2O were used for the experiments. Spectra were processed using the XWINNMR software (Bruker Biospin). For backbone assignments, a complete series of 2D side chain-selective experiments [11] and 3D triple resonance CBCA(CO)NH/CBCANH and HA(CACO)NH/HA(CA)NH spectra were used [12]. Side chain resonances were identified from 3D HBHA(CO)NH, H(CCCO)NH-TOCSY and (H)CC(CO)NH-TOCSY experiments in H_2O. Interproton distances for structure calculation were derived from a 2D NOESY (mixing time 60 ms), a 3D ^{15}N NOESY–HSQC (80 ms) both in 90% H_2O/10% D_2O, and a 3D ^{13}C HMQC–NOESY (80 ms) spectrum in 100% D_2O [12]. The SPARKY software was used for assignment [13].

^{15}N T_1 and T_2 relaxation data were measured as described previously [12]. Both T_1 and T_2 relaxation times were extracted from two series comprising each of 11 spectra with relaxation delays of 12, 52, 102, 152, 202, 302, 402, 602, 902, 2002 and 5002 ms for T_1 measurements and 6, 10, 18, 26, 34, 42, 82, 122, 162, 202 and 242 ms for T_2 measurements. Heteronuclear ^1H–^{15}N nuclear Overhauser effect (NOE) experiments were also recorded. Structures were calculated with the program ARIA 1.2 [14] using 113 manually assigned NOEs representing secondary structure NOE patterns, 18 hydrogen bonds and 19 dihedral angles derived from J_{HNHA}-modulated HMQC experiments [15]. After water refinement, the final ensemble was analysed by MOLMOL [16] and PROCHECK-NMR [17].

2.3. Kinetic binding experiments with cathepsins B, X and L

Human cathepsins B and X were expressed and purified as described previously [18,19]. The cDNA for human procathepsin L was amplified by PCR from a human placenta cDNA library (BD Biosciences Clontech, Palo Alto, CA) using gene-specific primers 5′-CCGCTCGAGAAAAGAGAGGCTGAAGCTACTCTAACATTTGATCACAGTTT-3′and 5′-ATTTGCGGCCGCTCACACAGTGGGGTAGCTGG-3′ and Expand DNA polymerase (Roche Applied Science, Mannheim, Germany). Cathepsin L was expressed and purified according to the procedure described for cathepsin B [18]. Kinetic experiments were performed as previously described [18]. Fluorescence was monitored on a SPEX FluoroMax spectrofluorometer (Jobin Yvon, Edison, NJ). All kinetic measurements were performed at 25°C in the presence of 50 mM sodium citrate, 1 mM EDTA, 2 mM DTT, 0.2 M NaCl and 3% DMSO. The assays for cathepsins B and L were carried out at pH 5.5 using the substrate carbobenzoxy-L-phenylalanyl-L-arginine-4-methylcoumarinyl-7-amide (Cbz-FR-MCA), for cathepsin X at pH 5.0 as described previously [19]. Inhibition studies were performed by measuring the steady-state rate of substrate hydrolysis (v_0) in the presence of G1-S2-p47(171–270). The type of inhibition and K_i values were determined by Dixon plot analysis, i.e., linear regression of reciprocal plots of the reaction rate ($1/v_0$ vs. [I]) at varying concentrations of substrate [20]. Statistical analyses were performed using the GraphPad Prism software (San Diego, CA).

2.4. NMR chemical shift mapping experiments with cathepsin L

A deuterated, ^{15}N-labelled sample of the SEP domain was prepared for interaction studies with unlabelled inactivated cathepsin L (see Section 2.1). Both proteins were dialysed against the same buffer comprising 20 mM NaP_i, 50 mM NaCl and 100 μM methyl methanethiosulfonate at pH 5.6 in 90% H_2O/10% D_2O. A ^{15}N HSQC spectrum was recorded immediately after addition of cathepsin L to the SEP domain using a Bruker DRX 600 MHz spectrometer equipped with a cryoprobe. Protein concentrations were kept minimal and the experimental temperature was kept low at 278 K to slow down the rapid proteolytic cleavage of the SEP domain construct which occurred at higher temperatures and protease concentrations. Final concentrations were 50 μM for the SEP domain and 10 μM for cathepsin L, respectively. Chemical shift perturbations were analysed using Sparky version 3.69.

3. Results and discussion

3.1. Solution structure of the human p47 SEP domain

A construct comprising residues G1-S2-p47(171–270) was used for structure determination by NMR. Resonance assignments were obtained for ^{13}C, ^{15}N and ^1H nuclei in all residues except for G1 and S2. The proton side chain resonances of Q174 and the aromatic ^{13}C, ^1H resonances of F249 and F252 could not be assigned. Structures were calculated using ARIA 1.2 [14] and refined iteratively by manual inspection of the NOESY spectra and repeated structure calculations. The final structures were based on approximately 1570 unambiguously assigned constraints, 18 hydrogen bonds and 19 dihedral angles derived from specific NOE patterns and J_{HNHA}-modulated experiments (Table 1).

The structure of the human p47 SEP domain construct (Figs. 1B and 2A) comprises a β-sheet composed of four strands (residues 180–187 (β1), 191–193 (β2), 198–200 (β3) 231–237 (β4)), and two α-helices (residues 207–215 (α1), 220–224 (α2)). One side of the β-sheet faces α1 and α2. The latter touches the end of β4 and β1 at the edge of the domain, arranged in a 90° angle with respect to α1. The hydrophobic core comprises residues V180, L184, L186, W187, F191, L193, L198, Y201, F209, L210, I213, L223, L225, V231, L233, M235 and F243. Only a small number of NOE distance restraints were observed for residues preceding D179 and following V244. The protein was well structured from residues D179 to V244. Residues more than 80% conserved in a non-redundant alignment of all SEP domains present in the SMART database are labelled green and black. The green-labelled residues L210, F209, F191, L198, W187 and F243 are located in a diagonal plane through the SEP domain, close to the loops between β1

Table 1
Structural statistics of the ensemble

Restraints	
ARIA output assignment for NOEs	
Unambiguous assignments	1570
Intra-residue	637
Sequential	330
Medium-range	165
Long-range	438
Ambiguous assignments	567
Others	
Manually assigned NOEs	113
H-Bonds (from NOE pattern)	18
Dihedrals (from NOE pattern and J_{HNHA} experiments)	19
Quality of the ensemble for 20 calculated structures	
RMSD (for residues 179-244): from MOLMOL	
Backbone atoms	1.04 ± 0.24 Å
Side chain heavy atoms	1.75 ± 0.27 Å
Violations:	
Distances >0.4 Å	0
Dihedrals > 5°	0
Ramachandran plot: (from PROCHECK NMR)	
Most favoured regions	80.9%
Additionally allowed regions	15.2%
Generously allowed regions	2.2%
Disallowed regions	1.8%

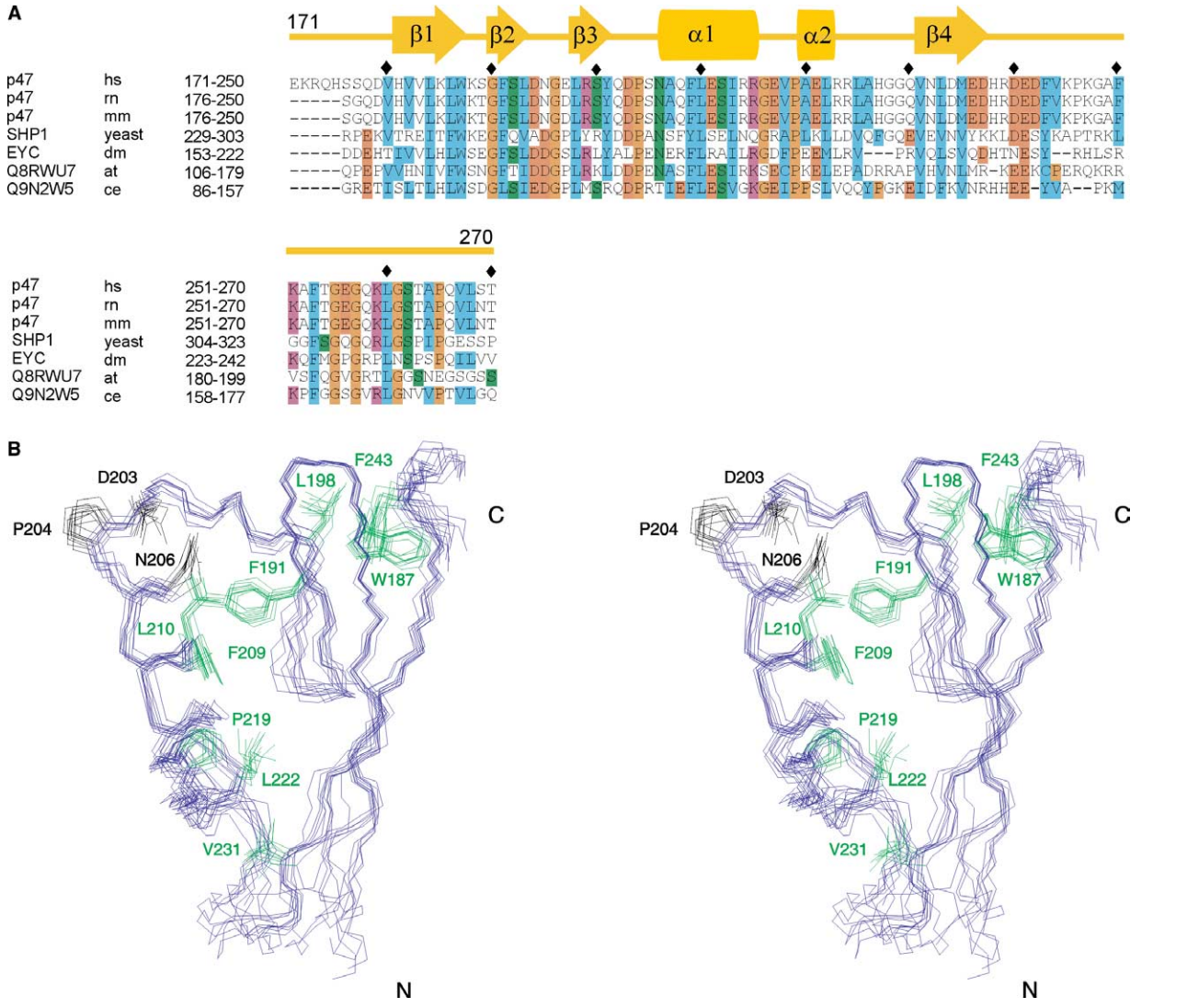

Fig. 1. (A) Multiple sequence alignment of selected SEP domains. The secondary structure is shown on top of the investigated SEP domain construct. The first two residues G1–S2 are not shown. Swissprot accession numbers from top to bottom: Q9UNZ2, O35987, Q9CZ44, P34223, Q8T4C3, Q8RWU7, Q9N2W5. The ruler (◆) starts at position 180 followed by 190, etc. (B) Ensemble of 10 lowest energy solution structures of the human p47 SEP domain. In green and black are the side chains of residues which are more than 80% conserved. Residues D203, P204 and N206 are found in a loop above a cross-sectional plane comprised by residues L210, F209, F191, L198, W187 and F243. Structural figures were generated using MOLMOL [16].

and β2 and before α1. F243 is less than 80% conserved but also shown, since it is found at the end of this plane near the flexible C-terminus. The black-labelled residues D203, P204 and N206 are found on the domain surface in a loop preceding α1 above the diagonal plane. Residues P219, L222 and V231 lie below this plane and are mainly involved in hydrophobic contacts between the β-sheet and α2. Yuan et al. [8] determined recently the structure of the rat p47 SEP domain (1VAZ). The overall structure of the human p47 SEP domain is the same but differs slightly in the orientation of the loop between α2 and β4 (Fig. 2A, highlighted in green). We assigned manually those NOEs which determine the loop orientation (available upon request from the authors). Our construct which did not contain a His tag showed NOEs which are indicative of contacts between the loop α2/β4 and strand β4. The potential binding site is well-ordered and very similar in both human and rat structures. The Cα RMSD of two lowest energy structures in this region (residues 179–195, 198–217 and 233–241) was 1.74 Å. Interestingly, no structural differences are caused by the three point mutations between the human and rat sequences. The mutation S189T is structurally neutral and the other two mutations appear in the flexible N-terminus.

The distribution of conserved hydrophobic residues and the calculated lipophilic and electrostatic potentials on the domain surface are shown in Fig. 2B–D. Residues F191, Y201, P204, L210, I213, P219, L222, L233 and M235 cover a continuous area (Fig. 2B, left). The surface on the reverse side (Fig. 2B, right) shows residues W187 and F243 making up one conserved area and the loop containing residues D203, P204 and N206 comprising a second. Residues V180, G196 and F209 are also shown. The lipophilic potential was calculated for the accessible surface area according to Heiden et al. [21]. Hydrophobic (yellow) and hydrophilic (green) areas are visualised in Fig. 2C and show sharp contours with cavities suitable for

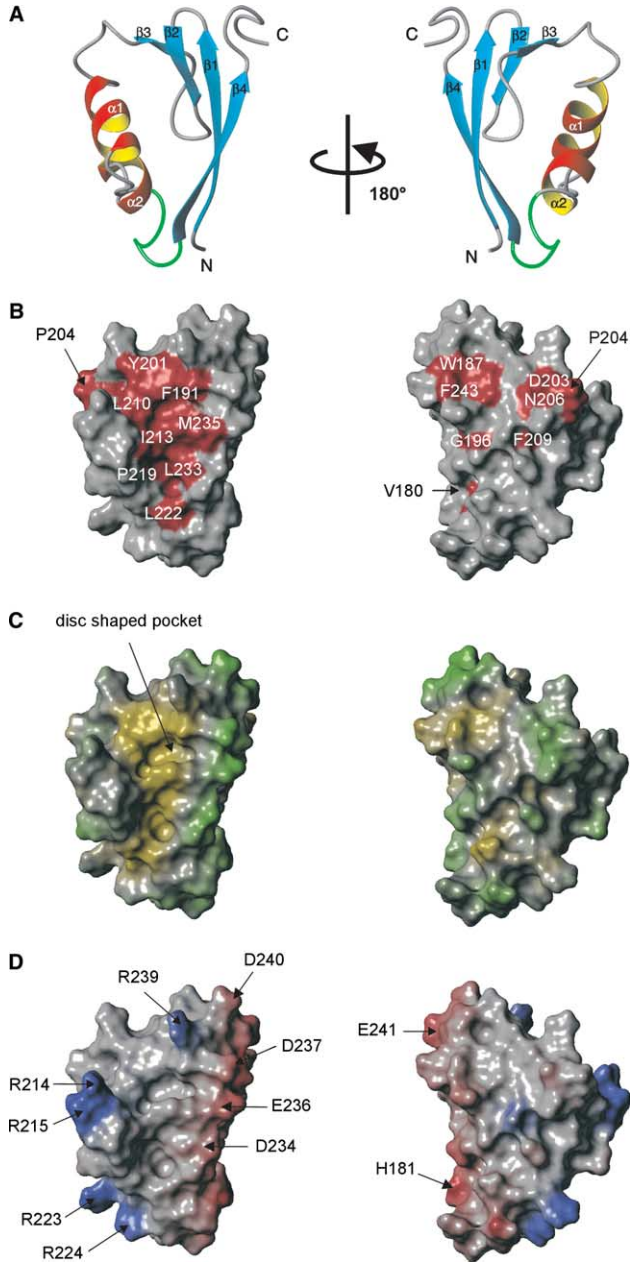

Fig. 2. (A) Ribbon representations of the human p47 SEP domain. (B–D) Surface properties of the human p47 SEP domain. The same orientations are used as in (A). (B) Surface exposed loop and conserved hydrophobic residues are shown in red. (C) Hydrophilic (green) and hydrophobic (yellow) regions. (D) Electrostatic potential: positive (blue), negative (red). All surface figures were made using SYBYL 6.9.

accommodating the side chains of interaction partners. This disc shaped pocket is large enough to bury a tryptophan side chain.

The electrostatic potential of the accessible surface area reveals a dipole character of the p47 SEP domain. Fig. 2D shows an acidic stretch, comprising residues D234, E236 and D237 from β4 and residues D240 and E241 from the C-terminal tail, on one side of the molecule. The basic residues R214, R215 from helix 1 and R223, R224 from helix 2 create a positive potential on the opposite side.

3.2. Dynamics of the investigated SEP construct G1-S2-p47(171–270)

The SEP domain boundaries were indicated in the SMART database as S176 and T270. Despite considerable sequence homology at the C-terminus, the structured region ends at V244. To investigate the flexibility of the C-terminus, we determined ^{15}N T_1, T_2 and heteronuclear NOEs (relaxation data not shown). The ratio T_1/T_2 drops significantly preceding residues D179 and following K245. The heteronuclear ^{1}H–^{15}N NOE measurements showed positive signals for the residues between D179 and K245, whereas the signals from the flexible termini were strongly negative. These data show that the N-terminal (G1-S2-p47(171–178)) and C-terminal (p47(245–270)) tails are therefore flexible in solution. The rotational correlation time τ_c was determined to be 6.4 ns, indicating a monomeric state for the domain under the conditions investigated.

Further experiments involving hydrogen exchange support the results of the relaxation measurements. After lyophilisation and redissolving in D_2O, we immediately measured ^{1}H–^{15}N HSQC experiments. Both flexible tails exchanged rapidly with D_2O. Amide protons from the structured regions were protected to varying extents. After 2 h, ^{15}N-attached protons from residues 182–187, 190–192, 199, 210–214, 222, 234, 236 and 238, which are located in the core, were not exchanged. In summary, the data from relaxation experiments and D_2O exchange, together with the number of assigned NOE restraints per residue, show the SEP domain to extend from residue D179 to V244.

3.3. A structure-derived hypothesis: The p47 SEP domain interacts with cysteine proteases

Neither the activity nor the cellular function of the p47 SEP domain is known to date. In light of the existing structural investigations and the biological context, we have developed a hypothesis based on the structural properties of two loops and the similarity of the overall structure of the SEP domain to inhibitors of cysteine proteases [22]. The p47 SEP domain has two very rigid and well-ordered loops (β1–β2, β3–α1), which are located close to the conserved residues of the protein core. The loop between β3 and α1 is particularly highly conserved. The C-terminus of the domain is close to these two loops, in particular to the loop connecting β1 and β2. Such arrangements are also seen in inhibitors of cysteine proteases, such as cystatins and stefins [23]. Due to the structural similarity, we hypothesised that the SEP domain may bind to and inhibit cysteine proteases.

We therefore investigated the inhibition of three cysteine proteases, cathepsins L, B and X, by the p47 SEP domain. The experiments showed clearly that G1-S2-p47(171–270) is a reversible competitive inhibitor of cathepsin L with a K_i of 1.5 μM (Fig. 3). Cathepsin B was much more weakly and cathepsin X not at all inhibited at the highest concentration of the SEP construct used (15 μM). The reduced or absent affinity of the SEP domain for cathepsins B and X ($K_i > 50$ μM) is likely to be due to unfavourable interactions with the occluding loop in cathepsin B [24] or the mini loop in cathepsin X [25].

NMR titration experiments were used to map the binding site between cathepsin L and the ^{15}N-labelled deuterated SEP domain. In agreement with our hypothesis, we observed chemical shift perturbations (CSP) for the amide proton and nitrogen resonances of residues S189 and G190 which are

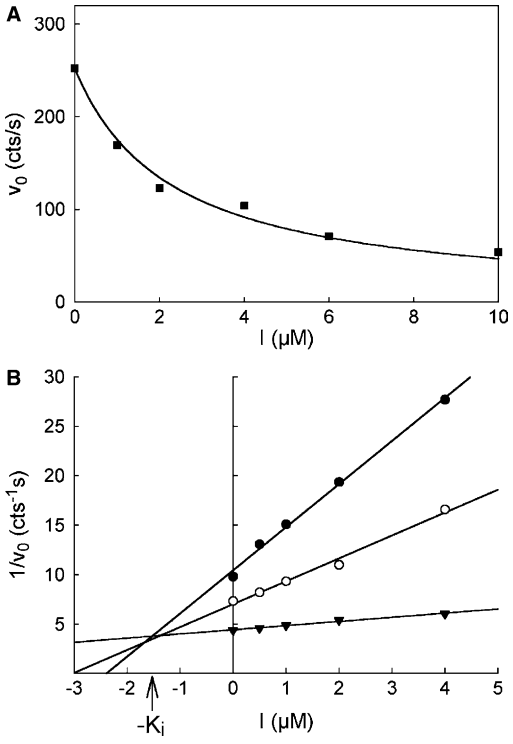

Fig. 3. Reversible competitive inhibition of human cathepsin L by the G1-S2-p47(171–270) SEP domain construct. (A) The rate of substrate hydrolysis (v_0) by cathepsin L was measured in the presence of varying amounts of the SEP domain. The rate of hydrolysis of the substrate Cbz-FR-MCA (1 μM) by cathepsin L (10 pM) was constant during the assay (15 min). (B) Dixon plots for the inhibition of cathepsin L by the SEP domain at 0.5 μM (●), 1 μM (○) and 4 μM (▼) of Cbz-FR-MCA. The K_i was determined from reciprocal plots ($1/v_0$) vs. [*I*] according to [20], and calculated to be 1.5 ± 0.2 μM.

located in the turn between β1 and β2, and for residues Y201, Q202, D203 and N206 found in the loop following β3. Additionally, we observed CSP near the flexible C-terminus particularly for residues F243 and K245. However, we conclude from the disappearance of the peaks due to F250, K251, T254, G255, E256, G257, L260, G261 and A264 that the C-terminus was cleaved.

Substrate-like cleavage of cystatins and reappearance of enzymatic activity after initial complex formation was previously described for cathepsin L [26]. Reappearance of enzyme activity after initial inhibition would result in a sigmoidal curve. We did not observe such temporary inhibition in the activity assay, presumably due to the low enzyme concentrations used. However, cleavage of the SEP domain by cathepsin L could still occur at higher enzyme concentrations or on prolonged incubation.

In conclusion, p47 may act as a specific adaptor molecule for cathepsin L to regulate a yet unidentified cellular process. Whether the SEP domain binds to cathepsin L in a chaperone-like manner or inhibits the activity of cathepsin L in vivo remains to be determined.

The structural coordinates have been deposited in the PDB under accession code 1SS6.

Acknowledgements: We are grateful for the financial support of this work by the BMBF-Leitprojekt "Strukturanalyse mit hohem Durchsatz für medizinisch relevante Proteine – Proteinstrukturfabrik" (Fk.01GG9812) and by the Friedrich-Baur-Stiftung (0031/2003).

References

[1] Ogura, T. and Wilkinson, A.J. (2001) Genes Cells 6, 575–597.
[2] Dreveny, I., Kondo, H., Uchiyama, K., Shaw, A., Zhang, X. and Freemont, P.S. (2004) EMBO J. 23, 1030–1039.
[3] Uchiyama, K., Jokitalo, E., Kano, F., Murata, M., Zhang, X., Canas, B., Newman, R., Rabouille, C., Pappin, D., Freemont, P. and Kondo, H. (2002) J. Cell. Biol. 159, 855–866.
[4] Dieckmann, T., Withers-Ward, E.S., Jarosinski, M.A., Liu, C.F., Chen, I.S.Y. and Feigon, J. (1998) Nat. Struct. Biol. 5, 1042–1047.
[5] Buchberger, A. (2002) Trends Cell Biol. 12, 216–221.
[6] Yuan, X., Shaw, A., Zhang, X., Kondo, H., Lally, J., Freemont, P.S. and Matthews, S. (2001) J. Mol. Biol. 311, 255–263.
[7] Schultz, J., Copley, R.R., Doerks, T., Ponting, C.P. and Bork, P. (2000) Nucleic Acids Res. 28, 231–234.
[8] Yuan, X., Simpson, P., McKeown, C., Kondo, H., Uchiyama, K., Wallis, R., Dreveny, I., Keetch, C., Zhang, X., Robinson, C., Freemont, P. and Matthews, S. (2004) EMBO J. 23, 1463–1473.
[9] Bussow, K., Nordhoff, E., Lubbert, C., Lehrach, H. and Walter, G. (2000) Genomics 65, 1–8.
[10] Labudde, D., Leitner, D., Schmieder, P. and Oschkinat, H. (2002) BRUKER-Report 150, 8–11.
[11] Schubert, M., Smalla, M., Schmieder, P. and Oschkinat, H. (1999) J. Magn. Reson. 141, 34–43.
[12] Kay, L.E. (1997) Biochem. Cell Biol. 75, 1–15.
[13] Goddard, T.D. and Keller, D.G. (2002) University of California, San Francisco, CA.
[14] Linge, J., Habeck, M., Rieping, W. and Nilges, M. (2003) Bioinformatics 19, 315–316.
[15] Billeter, M., Neri, D., Otting, G., Qian, Y.Q. and Wuthrich, K. (1992) J. Biomol. NMR 2, 257–274.
[16] Koradi, R., Billeter, M. and Wuthrich, K. (1996) J. Mol. Graph 14, 51–55, 29–32.
[17] Laskowski, R.A., Rullmannn, J.A., MacArthur, M.W., Kaptein, R. and Thornton, J.M. (1996) J. Biomol. NMR 8, 477–486.
[18] Nagler, D.K., Storer, A.C., Portaro, F.C., Carmona, E., Juliano, L. and Menard, R. (1997) Biochemistry 36, 12608–12615.
[19] Nagler, D.K., Zhang, R., Tam, W., Sulea, T., Purisima, E.O. and Menard, R. (1999) Biochemistry 38, 12648–12654.
[20] Dixon, M. (1953) Biochem. J. 55, 170–171.
[21] Heiden, W., Moeckel, G. and Brickmann, J. (1993) J. Comput. Aided Mol. Des. 7, 503–514.
[22] Stubbs, M.T., Laber, B., Bode, W., Huber, R., Jerala, R., Lenarcic, B. and Turk, V. (1990) EMBO J. 9, 1939–1947.
[23] Jenko, S., Dolenc, I., Guncar, G., Dobersek, A., Podobnik, M. and Turk, D. (2003) J. Mol. Biol. 326, 875–885.
[24] Musil, D., Zucic, D., Turk, D., Engh, R.A., Mayr, I., Huber, R., Popovic, T., Turk, V., Towatari, T. and Katunama, N. (1991) EMBO J. 10, 2321–2330.
[25] Sivaraman, J., Nagler, D.K., Zhang, R., Menard, R. and Cygler, M. (2000) J. Mol. Biol. 295, 939–951.
[26] Machleidt, W., Nagler, D.K., Assfalg-Machleidt, I., Stubbs, M.T., Fritz, H. and Auerswald, E.A. (1995) FEBS Lett. 361, 185–190.